Large-amplitude electrostatic waves associated with magnetic ramp substructure at Earth's bow shock

A. J. Hull,[1] D. E. Larson,[1] M. Wilber,[1] J. D. Scudder,[2] F. S. Mozer,[1] C. T. Russell,[3] and S. D. Bale[1]

Received 20 December 2005; revised 25 April 2006; accepted 15 June 2006; published 3 August 2006.

[1] We present Polar observations of high frequency (100 Hz $\lesssim f \lesssim$ 4000 Hz) electrostatic (ES) waves at Earth's bow shock under extreme solar wind conditions. Although solitary waves are observed, the most prevalent structures in the magnetic ramp are coherent, large-amplitude (up to 80 mV/m) ES wave packets, which last 10–30 cycles, and propagate at varied obliquities relative to the magnetic field. The ES wave power is well correlated with maxima in the magnetic ramp substructure, suggesting that these maxima are important source regions. Detailed interferometric based analysis of waveforms show that they have wavelengths of a few hundred meters (e.g., $\sim 20\lambda_D \sim 0.5\rho_e$) and phase speeds at the acoustic speed, suggesting that they are ion acoustic waves (IAW)s. The IAWs, having potentials $\lesssim$1 V with no net change, are not likely to affect bulk plasma energization, though they may scatter the plasma and thus affect plasma thermalization. **Citation:** Hull, A. J., D. E. Larson, M. Wilber, J. D. Scudder, F. S. Mozer, C. T. Russell, and S. D. Bale (2006), Large-amplitude electrostatic waves associated with magnetic ramp substructure at Earth's bow shock, *Geophys. Res. Lett.*, *33*, L15104, doi:10.1029/2005GL025564.

1. Introduction

[2] Plasma waves and their role in irreversible plasma heating in shock transitions have been extensively studied. Nonetheless, the microphysical processes that thermalize the plasma are still not fully understood. Early observational studies [e.g., and references therein *Gurnett*, 1985], based on intermittently sampled power spectra, have identified the shock ramp as the region where wave power is most intense. The wave spectrum usually consists of a low-frequency electromagnetic (EM) component, believed to be whistler waves, and an electrostatic component above a few 100 Hz, characterized by a broad spectrum that peaks near $\sim$1 kHz. The ES component is thought to be composed of ion acoustic waves, but without rest frame frequencies and wavelengths the identity of these waves was difficult to establish. Recent waveform observations revealed that the electrostatic component is coherent and composed of bipolar electrostatic solitary waves (ESW), and electrostatic quasi-monochromatic wave structures (EQMW), often called ion-acoustic like waves [e.g., *Matsumoto et al.*, 1998; *Bale et al.*, 1998]. From 2D electric waveform measurements, *Bale et al.* [1998] determined the scales ($\sim\lambda_{De}$) and identified ESWs consistent with 1D BGK electron phase space holes. The scales, polarization and thus the identity of EQMW are not well-established. Also, these waves, due to short sample durations, could not be placed in full context with the shock magnetic ramp structure, on which is often superposed large amplitude ($\delta B/B \sim 1$) quasistationary structure having length scales $\sim 0.1\, c/\omega_{pi}$ [*Newbury et al.*, 1998].

[3] Here we present long-duration Polar observations of waveforms in the ramp of Earth's bow shock. While we include electric and magnetic fields from DC to 8000 Hz, we focus on electrostatic waves occurring at frequencies near 100 Hz to a few thousand Hz. The Polar electric field instrument (EFI) provides the first 3-axis measurements across the shock, allowing for a better evaluation of the shock electric fields than possible from 2-axis instruments. Of interest are the amplitudes, scales and obliquities of these ES waves, which we place in context with the shock ramp internal structure for the first time.

2. Instrumentation and Observations

[4] Polar/EFI [*Harvey et al.*, 1995] consists of three orthogonal sphere pairs; two pairs lie in the spin plane with separations of 130 m and 100 m, and a third pair is separated by 14 m along the spin axis. The search coil magnetic field measurements were made by the Plasma Wave Instrument [*Gurnett et al.*, 1995]. This study focuses on electric field and search coil magnetic field data collected by EFI in 1600 Hz and 8000 Hz burst mode samples. EFI provides three pairs of probe to spacecraft skin potential difference data, which permit the use of interferometry to yield wave speeds and wavelengths. For context, we used 8 Hz magnetic field data from the magnetic field experiment [*Russell et al.*, 1995] and electron and ion moment data from the Hydra instrument [*Scudder et al.*, 1995]. We also used densities obtained from EFI 2.5 Hz spacecraft potential data (via a density-potential relation established for the current epoch), which agree with Hydra moments to within 35%.

[5] Since time delays are not always well resolved on all three orthogonal probe baselines, we used the method described by *Hoppe and Russell* [1983] to get waveform wavelengths, rest frame frequencies, and phase speeds. The method requires the wave normal vector $\hat{\mathbf{k}}_{GSM}$, which was obtained from a maximum variance analysis (MVA) applied to the electric field. We used the resolved wave motion along the probe baselines to remove the 180° ambiguity in

[1]Space Science Laboratory, University of California, Berkeley, California, USA.
[2]Department of Physics and Astronomy, University of Iowa, Iowa City, Iowa, USA.
[3]Institute of Geophysics and Planetary Physics, University of California, Los Angeles, California, USA.

0094-8276/06/2005GL025564$05.00

$\hat{\mathbf{k}}_{GSM}$. Electric field amplitudes were corrected for interference errors associated with the finite motion of short wavelength waves across a probe baseline [*Angelopoulos et al.*, 2001], prior to computing $\hat{\mathbf{k}}_{GSM}$.

[6] Below we present results from a detailed analysis of ES waves (satisfying E/B $\gtrsim$ c) observed at frequencies from $\sim$100 Hz to a few thousand Hz in the magnetic ramp of two bow shock crossings. The upstream conditions and shock geometries differ for each event. Such ES waves have been presented in earlier studies [e.g., *Gurnett*, 1985; *Matsumoto et al.*, 1998, and references therein], but this study benefits from the unique complement of long-duration, high-time resolution, three axis AC electric and magnetic field waveform data provided by Polar.

[7] Figure 1 shows data observed by Polar during an outbound pass through Earth's bow shock at $\sim$1957 UT on April 08, 2001, at a location near the nose ($\mathbf{R}_{GSM}$ = (8.9, −1.9, 0.4)). The shock is quasi-perpendicular (θ_{Bn} = 88°), with $\beta \sim 0.55$, and is characterized by unusually high solar wind flow ($V_{SW} \sim$ 800 km s^{-1}), yielding an upstream Fast mode number $M_F = U_n/C_F \sim 8$ (U_n is the shock rest frame normal flow and C_F is the Fast mode speed). The shock normal determined by the *Viñas and Scudder* [1986] method is $\hat{\mathbf{n}}$ = (0.9940, −0.003, −0.110), with an angular uncertainty of 5°. The electron and ion temperature changes (ΔT_e = 110 eV and $\Delta T_i \sim$ 950 eV) are unusually large. The shock ramp has considerable fine structure with multiple maxima occurring in the magnetic field (Figure 1a) and density (Figure 1b). This structure with a period of $\sim$0.8 s is not an artifact of the spacecraft (spin period 6 s).

[8] Vertical lines in Figure 1 delimit a region where all three components of the electric and magnetic waveforms were sampled at a 1600 Hz burst rate. Omnidirectional dynamic power spectra of burst electric and magnetic fields are shown in Figures 1c–1d, respectively. The power spectral densities have been multiplied by frequency f to emphasize structure at higher frequencies. These rescaled power spectra represent to within a constant factor the contribution to the total integrated power at a given time (e.g., $P_E^{tot}(t) = \Delta x \sum P_E(f, t)f$, where the spacing $\Delta x = \Delta f/f$ is by construction a fixed constant in the continuous wavelet transform applied to the signal). In Figures 1c–1d an abrupt burst of electric and magnetic field occurs within the shock layer. In the magnetic pedestal ($\sim$1957:03.5–1957:07 UT) much of the power is below 50 Hz, originating from lower frequency whistler waves extensively discussed in the literature [e.g., *Gurnett*, 1985, and references therein]. Nearly monochromatic bursts of EM waves (light blue) are also observed near 200 Hz in the pedestal region. These waves, which are right hand polarized whistlers that are oblique to the background magnetic field unit vector $\hat{\mathbf{b}}$, may be the shock analogue of lion roars observed in the magnetosheath in association with mirror mode waves. Bursts of broadband ES waves of small amplitude ($\lesssim$10 mV/m) are also seen. With increasing penetration into the shock ramp and overshoot region the intensity of the electric and magnetic fields increases. Intense broadband electric field activity with no magnetic field component is observed to occur near and above 100 Hz, intermittently throughout the ramp.

[9] Figures 1e–1g show the amplitude perpendicular to $\hat{\mathbf{b}}$, the parallel amplitude, and the downsampled average power of the burst electric waveforms above 100 Hz, respectively. Although there are small contributions from EM waves (a few mV/m), the power is dominated by the intense ES waves at these frequencies. The total ES wave amplitudes are quite varied in the interval, reaching 75–80 mV/m. Contrary to early studies [e.g., *Rodriquez and Gurnett*, 1975], the ES waves are not generally field-aligned, but have varied obliquities. The ES wave power above 100 Hz shows enhancements collocated with local maxima in the DC magnetic field (Figure 1h).

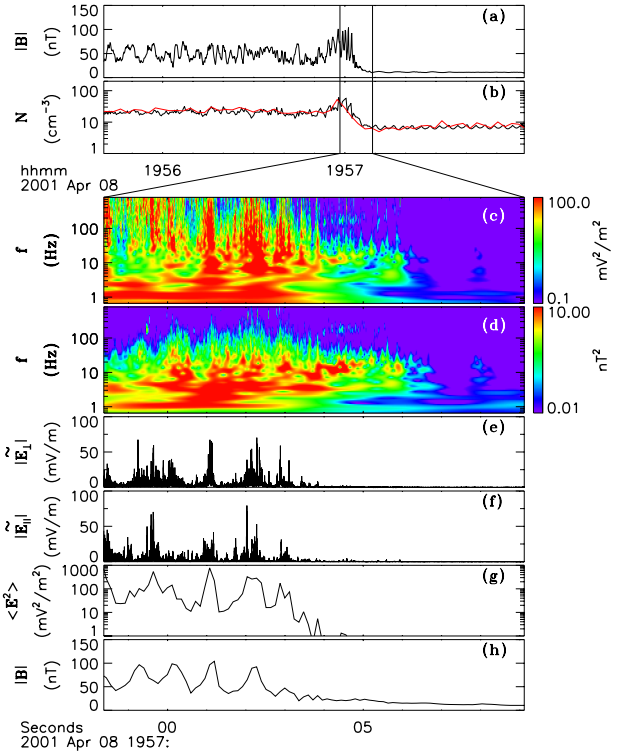

Figure 1. Plasma and field data observed at a strong, perpendicular bow shock on April 08, 2001 by Polar. (a) Magnetic field amplitude sampled at 8 Hz. (b) 2.5 Hz spacecraft potential density estimates (black curve) and 1s Hydra electron densities (red curve) sampled every two seconds. Vertical lines in Figures 1a and 1b indicate an interval where the electric and magnetic fields were sampled at 1600 Hz. (c–d) Rescaled dynamic power spectra of burst sampled E and B. (e–f) The perpendicular and parallel electric fields above 100 Hz. (g) The average power of the electric field above 100 Hz. The electric field power was boxcar averaged down to 0.125 sec resolution prior to interpolation onto the 8 Hz magnetic field time tags. (h) The magnetic field for context.

[10] Many of the waveforms in the burst interval appear to be large amplitude ES wave packets, which at times are accompanied by ESW structures. As an example, the three components of the electric field high-pass filtered at 100 Hz in field-aligned coordinates (FAC) are shown in Figures 2a–2c. The FAC system is defined by $\hat{\mathbf{e}}_{\perp 1} \equiv \hat{\mathbf{v}}_{sc} \times \hat{\mathbf{b}}/|\hat{\mathbf{v}}_{sc} \times \hat{\mathbf{b}}|$, $\hat{\mathbf{e}}_{\perp 2} \equiv \hat{\mathbf{b}} \times \hat{\mathbf{e}}_{\perp 1}/|\hat{\mathbf{b}} \times \hat{\mathbf{e}}_{\perp 1}|$, $\hat{\mathbf{b}}$, where $\hat{\mathbf{v}}_{sc}$ $\hat{\mathbf{v}}_{sc}$ is the spacecraft velocity unit vector. The rather varied waveform amplitude occasionally reaches 50 mV/m. The waveform lies in the plane defined by $\hat{\mathbf{b}}$ and $\hat{\mathbf{e}}_{\perp 2}$,

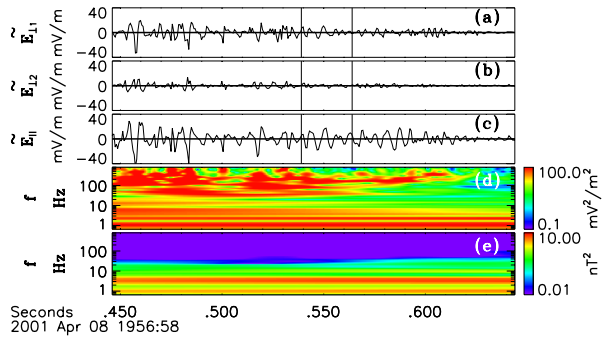

Figure 2. (a–c) Electric fields in a FAC system. (d–e) Rescaled dynamic power spectra of **E** and **B**.

and is characterized by a typical $E_{\parallel}/E_{\perp}$ ratio of 1.6. The electric field power spectrum (not shown) peaks at ~160 Hz and the associated E/B ratio is greater than the speed of light, verifying that the waveform is electrostatic. In the interval bounded by vertical lines in Figure 2a, we found $\hat{\mathbf{k}}_{\mathrm{GSM}}$ = (0.050, −0.593, −0.804), which is at an angle θ_{kB} = 22° relative to the local magnetic field and is nearly in the shock plane (θ_{kn} = 82°). The delay time (1.1×10^{-3} s) was determined by cross-correlating the 130 m spin plane pair of opposing probe to skin potential measurements, high-pass filtered at 100 Hz. Using an effective boom length of 65 m and an angle between the boom vector and $\hat{\mathbf{k}}_{\mathrm{GSM}}$ of 47°, we determined a wavelength of $\lambda \sim 260 \pm 90$ m = $16\lambda_D = 0.5\rho_e$ (λ_D is the Debye length and ρ_e is the electron gyroradius, estimated from a spacecraft potential density N_{ϕ} = 27 cm^{-3}, electron temperature T_e = 140 eV and magnetic field B = 52.7 nT). With a bulk velocity of $\mathbf{U}_{\mathrm{GSM}}$ = (−470, 90, 50) km s^{-1}, the plasma rest frame frequency was found to be f_r = 600 Hz, which is below the ion plasma frequency ($f_{pi} \sim 1$ kHz). The phase speed V_{ph} = 160 ± 70 km s^{-1} agrees with the ion acoustic speed $C_{ia} \equiv \sqrt{(T_e + 3T_i)/m_i}$ = 240 ± 75 km s^{-1} (ion temperature T_i = 160 eV). These results suggest that this is an IAW.

[11] Using the same format as Figure 1, Figure 3 shows data at a quasi-parallel shock (θ_{Bn} = 40°) observed on March 30, 2002. This event is characterized by an upstream flow $V_{SW} \sim 500$ km s^{-1}, $M_F \sim 5$, and $\beta \sim 2.5$. The shock normal is $\hat{\mathbf{n}}$ = (0.939, −0.063, 0.338). All components of the electric and magnetic fields were sampled at 8 kHz in the region indicated by the vertical lines in Figure 3. At frequencies below 100 Hz, the waveforms are primarily electromagnetic. With few exceptions, waves near and above 100 Hz are electrostatic. This is evident from the green to red signatures in the rescaled power spectra of the electric field (Figure 3c), which has no apparent magnetic field counterpart (Figure 3d). The wave amplitudes, reaching 20–30 mV/m, are not as large as was seen in the previous case, which may be indicative of dependencies on shock conditions, such as geometry, Mach number or β. Although there are instances where the parallel component dominates the signal (e.g., ~0500:31 UT, ~0500:33 UT, ~0500:34 UT), waveforms with a significant perpendicular electric field component are seen throughout the interval (Figures 3e–3f), suggesting oblique ES wave propagation. As in the previous example, the average ES wave power

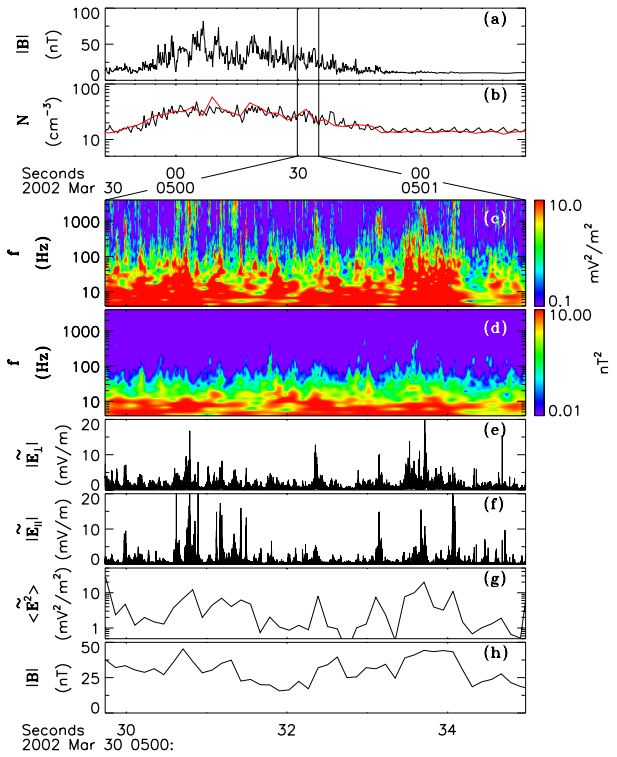

Figure 3. Burst electric and magnetic field data at a quasi-parallel bow shock observed on March 30, 2002 by Polar (same format as Figure 1).

shown in Figure 3g is generally well correlated with maxima in the DC magnetic field (Figure 3h).

[12] The most prevalent ES waveforms in the interval are wave packets lasting 10–30 cycles, which at times are embedded with ESWs. Many of these packets appear to be short scale IAWs. Figure 4 (same format as Figure 2) shows a pair of nonlinear parallel ES wave packets, with amplitudes reaching 20 mV/m. The packet durations last ten wave cycles, corresponding to an envelope length scale of $\sim 5\rho_e$. The waveforms are field-aligned and characterized by a typical ratio $E_{\parallel}/E_{\perp}$ = 8.4. In the interval indicated by vertical lines in Figure 4, MVA yielded $\hat{\mathbf{k}}_{\mathrm{GSM}}$ = (−0.361, 0.931, 0.056), with θ_{kB} = 3° and θ_{kn} = 110°. The wave has a wavelength λ = 230 ± 140 m (=$23\lambda_D = 0.5\rho_e$) and plasma rest frame frequency f_r = 0.9 ± 0.3 kHz, yielding a phase speed of V_{ph} = 200 ± 100 km s^{-1}. Here f_{pi} = 1.0 kHz, f_{ce} =

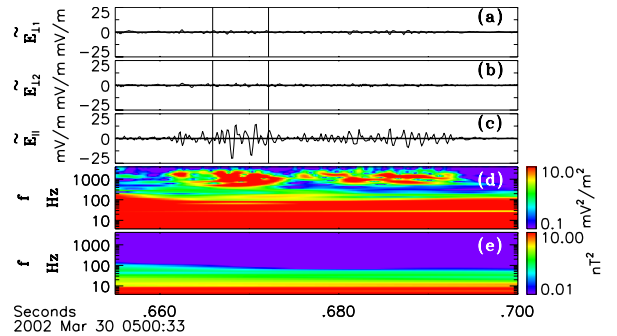

Figure 4. (a–c) Electric fields in a FAC system. (d–e) Rescaled dynamic power spectra of **E** and **B**.

1.2 kHz, and C_{ia} = 300 ± 100 km s^{-1}, given a magnetic field B = 43 nT, N_ϕ = 24 cm^{-3}, T_e = 56 eV and T_i = 250 eV. These results suggest that the wave is an IAW.

[13] An example of a large-amplitude ES wave packet propagating obliquely to the magnetic field in the shock ramp is given in Figure 5 (same format as Figure 2). The packet duration lasts ~30 wave periods, which corresponds to a length scale of 9 ρ_e. The waveform, with an amplitude reaching ~40 mV/m, has a dominant perpendicular component ($E_\parallel/E_\perp$ = 0.55). The wave normal is $\hat{\mathbf{k}}_{GSM}$ = (−0.382, −0.563, −0.733), with θ_{kB} = 113° and θ_{kn} = 125°. The wavelength and rest frame frequency are found to be λ = 130 ± 60 m (= 13λ_D = 0.3ρ_e) and f_r = 2.4 ± 1.3 kHz, yielding a phase speed of V_{ph} = 300 ± 200 km s^{-1}. Given B = 44 nT, N_ϕ = 26 cm^{-3}, T_e = 55 eV and T_i = 250 eV, we estimated f_{pi} = 1.1 kHz, f_{ce} = 1.2 kHz, and C_{ia} = 300 ± 100 km s^{-1}. These results are consistent with an IAW description.

3. Discussion and Conclusions

[14] We have presented two shock crossings where the electrostatic wave power above 100 Hz was significantly enhanced at or near magnetic field local maxima within the shock ramp. This correlation suggests that these maxima are important sites for the generation of these waves, placing important constraints on viable production mechanisms. The ES waves are not generally field-aligned, but have quite varied obliquities. A preliminary survey of ES waveforms above 100 Hz occurring in the shocks presented here suggests that many are IAWs. However, they often occur under conditions where $T_e \sim T_i$, and at magnetic field maxima as opposed to where their gradients are maxima, for which homogeneous linear theory predicts these waves should be strongly damped. The driven nature of the shock system may facilitate the excitation of IAWs nonetheless, but they may be restricted to exist close to their source location.

[15] A possible source may be from non-Maxwellian electron distributions. *Thomsen et al.* [1983] showed that short scale, parallel IAWs can be excited from field-aligned electron beams in the ramp. Here we give a slightly different mechanism. Theoretically, the adiabatic Vlasov mapping of electrons in the DC electric and magnetic fields predicts distortions/voids in the electron velocity space distributions, which must be filled to connect Hugoniot states [e.g., *Hull et al.*, 2001, and references therein]. These phase space voids should be largest where the electric potentials are maximized — where the magnetic fields are strongest. The voids yield double humped reduced distribution functions, which are expected to be unstable to short wavelength electrostatic waves, including the IAWs presented here.

[16] The IAWs are not expected to significantly affect the bulk plasma energization process, since the wave potentials are oscillatory with amplitudes ($\lesssim$1 V) much smaller than the shock DC potential, and have no apparent net potential drop. The IAWs may play a role in scattering ions, and owing to their short scale ($k\rho_e \gg 1$), and low phase speeds ($\omega/kv_e \ll 1$, where v_e is the electron thermal speed), may be the mechanism responsible for scattering electrons into inaccessible regions of phase space and hence form observed flat-topped electron distributions [*Feldman et al.*, 1982].

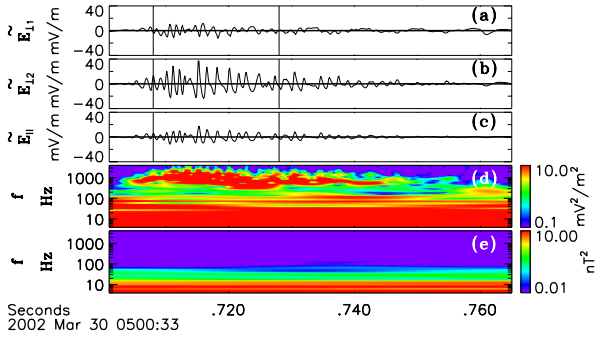

Figure 5. (a–c) Electric fields in a FAC system. (d–e) Rescaled dynamic power spectra of **E** and **B**.

[17] **Acknowledgment.** Work was supported by NASA grants NAG5-11733 and NNG05GC28G at UC Berkeley and University of Iowa, respectively.

References

Angelopoulos, V., et al. (2001), Wave power studies of cusp crossings with the Polar satellite, *J. Geophys. Res.*, *106*, 5987–6006.

Bale, S. D., P. J. Kellogg, D. E. Larson, R. P. Lin, K. Goetz, and R. P. Lepping (1998), Bipolar electrostatic structures in the shock transition region: Evidence of electron phase space holes, *Geophys. Res. Lett.*, *25*, 2929–2932.

Feldman, W. C., S. J. Bame, S. P. Gary, J. T. Gosling, D. J. McComas, and M. F. Thomsen (1982), Electron heating within the Earth's bow shock, *Phys. Rev. Lett.*, *49*, 199–201.

Gurnett, D. A. (1985), Plasma waves and instabilities, in *Collisionless Shocks in the Heliosphere: Reviews of Current Research*, *Geophys. Monogr. Ser.*, vol. 35, edited by B. T. Tsurutani and R. G. Stone, pp. 207–224, AGU, Washington, D. C.

Gurnett, D. A., et al. (1995), The Polar plasma wave instrument, *Space Sci. Rev.*, *71*, 597–622.

Harvey, P., et al. (1995), The electric field instrument on the Polar satellite, *Space Sci. Rev.*, *71*, 583–596.

Hoppe, M. M., and C. T. Russell (1983), Plasma rest frame frequencies and polarizations of low-frequency upstream waves: ISEE 1 and 2 observations, *J. Geophys. Res.*, *88*, 2021–2028.

Hull, A. J., J. D. Scudder, D. E. Larson, and R. P. Lin (2001), Electron heating and phase space signatures at supercritical, fast mode shocks, *J. Geophys. Res.*, *106*, 15,711–15,733.

Matsumoto, H., H. Kojima, and Y. Omura (1998), Plasma waves in geospace: GEOTAIL observations, in *New Perspectives on the Earth's Magnetotail*, *Geophys. Monogr. Ser.*, vol. 105, edited by A. Nishida, D. N. Baker, and S. W. H. Cowley, pp. 259–319, AGU, Washington, D. C.

Newbury, J. A., C. T. Russell, and M. Gedalin (1998), The ramp widths of high-Mach-number, quasi-perpendicular collisionless shocks, *J. Geophys. Res.*, *103*, 29,581–29,593.

Rodriquez, P., and D. A. Gurnett (1975), Electrostatic and electromagnetic turbulence associated with the Earth's bow shock, *J. Geophys. Res.*, *80*, 19–31.

Russell, C. T., et al. (1995), The GGS/Polar magnetic fields investigation, *Space Sci. Rev.*, *71*, 563–582.

Scudder, J., et al. (1995), Hydra- a three-dimensional electron and ion hot plasma instrument for the Polar spacecraft of the GGS mission, *Space Sci. Rev.*, *71*, 459–495.

Thomsen, M. F., S. P. Gary, W. C. Feldman, T. E. Cole, and H. C. Barr (1983), Stability of electron distributions within the Earth's bow shock, *J. Geophys. Res.*, *88*, 3035–3045.

Viñas, A. F., and J. D. Scudder (1986), Fast and optimal solution to the Rankine-Hugoniot problem, *J. Geophys. Res.*, *91*, 39–58.

S. D. Bale, A. J. Hull, D. E. Larson, F. S. Mozer, and M. Wilber, Space Science Laboratory, University of California, 7 Gauss Way, Berkeley, CA 94720, USA. (ahull@ssl.berkeley.edu)

C. T. Russell, Institute of Geophysics and Planetary Physics, University of California, Los Angeles, CA 90095, USA.

J. D. Scudder, Department of Physics and Astronomy, University of Iowa, Iowa City, IA 52242, USA.